PAPER

Neutron spectroscopy measurements of 14 MeV neutrons at unprecedented energy resolution and implications for deuterium–tritium fusion plasma diagnostics

To cite this article: D Rigamonti *et al* 2018 *Meas. Sci. Technol.* **29** 045502

View the article online for updates and enhancements.

Neutron spectroscopy measurements of 14 MeV neutrons at unprecedented energy resolution and implications for deuterium–tritium fusion plasma diagnostics

D Rigamonti[1,2] , L Giacomelli[2], G Gorini[1,2], M Nocente[1,2] , M Rebai[1,2],
M Tardocchi[2], M Angelone[3], P Batistoni[3], A Cufar[4], Z Ghani[5], S Jednorog[6],
A Klix[7], E Laszynska[6], S Loreti[3], M Pillon[3], S Popovichev[5], N Roberts[8],
D Thomas[8] and JET Contributors*

EUROfusion consortium, Culham Science Centre, Abington, United Kingdom

[1] Dipartimento di Fisica 'G. Occhialini', Università degli Studi di Milano-Bicocca, Milano, Italy
[2] Istituto di Fisica del Plasma 'P. Caldirola', CNR, Milano, Italy
[3] ENEA, I-00044 Frascati, Rome, Italy
[4] Jozef Stefan Institute, Jamova cesta 39, 1000, Ljubljana, Slovenia
[5] CCFE, Abingdon, Oxon, OX14 3DB, United Kingdom
[6] Institute of Plasma Physics and Laser Microfusion, Hery 23, 01-497 Warsaw, Poland
[7] Karlsruhe Institute of Technology, 76344 Eggenstein-Leopoldshafen, Karlsruhe, Germany
[8] National Physical Laboratory, Teddington, TW11 OLW, United Kingdom

E-mail: davide.rigamonti@mib.infn.it

CrossMark

Abstract

An accurate calibration of the JET neutron diagnostics with a 14 MeV neutron generator was performed in the first half of 2017 in order to provide a reliable measurement of the fusion power during the next JET deuterium–tritium (DT) campaign. In order to meet the target accuracy, the chosen neutron generator has been fully characterized at the Neutron Metrology Laboratory of the National Physical Laboratory (NPL), Teddington, United Kingdom. The present paper describes the measurements of the neutron energy spectra obtained using a high-resolution single-crystal diamond detector (SCD). The measurements, together with a new neutron source routine 'ad hoc' developed for the MCNP code, allowed the complex features of the neutron energy spectra resulting from the mixed D/T beam ions interacting with the T/D target nuclei to be resolved for the first time. From the spectral analysis a quantitative estimation of the beam ion composition has been made. The unprecedented intrinsic energy resolution ($<1\%$ full width at half maximum (FWHM) at 14 MeV) of diamond detectors opens up new prospects for diagnosing DT plasmas, such as, for instance, the possibility to study non-classical slowing down of the beam ions by neutron spectroscopy on ITER.

Keywords: neutron spectroscopy, diamond detectors, plasma diagnostics, 14 MeV neutron generator

(Some figures may appear in colour only in the online journal)

---

* See the author list of [23].

1. Introduction

The Joint European Torus (JET) is the largest experimental fusion device in the world and currently is the only one that can operate with tritium. It is equipped with several neutron diagnostics [1], in particular fission chambers (KN1) and in-vessel activation system (KN2), both able to measure the absolute neutron emission rate over the whole range from 10^8 n s^{-1} up to 10^{19} n s^{-1} in deuterium–tritium (DT) plasma scenarios. An accurate calibration of both KN1 and KN2 with 14 MeV neutrons is needed in order to provide reliable measurements of the neutron yield and of the fusion power during the next DT campaign planned in 2019 [2]. The neutron calibration consists in placing a neutron source of known intensity and energy spectrum at different positions inside the tokamak vessel and recording the KN1 and KN2 signals. The chosen neutron source was a 14 MeV neutron generator (NG) type ING-17 provided by VNIIA [3]. Two nominally identical neutron generators (NG#1 and NG#2) have been procured to mitigate the risk of failure. In the NGs, a mixed $D_x^+/T_x^+/D_xT_y^+$ beam (nominally 50–50%, $x, y = 1, 2$) is accelerated at a nominal energy of 100 keV onto a titanium target containing T/D (nominally 50–50%) inside a sealed tube. The NG thus produces 14 MeV neutron beam-target fusion reactions [4].

In order to meet the calibration target accuracy of 10% on KN1 and KN2, the two NGs have been fully characterized and calibrated at the Neutron Metrology Laboratory of the National Physical Laboratory (NPL, Teddington, UK). Two experimental campaigns were performed in November 2015 and June 2016 and aimed at determining the neutron emission rate and spectrum as a function of the angle of observation for both NGs. The NGs were placed at the centre of the low-scatter area of the accelerator hall which is equipped with rotating arms so that simultaneous measurements with several types of detectors at different angles with respect to the NG were possible. In this experiment a liquid scintillator detector (NE213), a long counter, activation foils and single crystal diamond detectors were used. The whole calibration and characterization campaign is described in [4].

For carrying out the data analysis and to simulate the NG neutron emission spectra a neutron source routine has been developed with the MCNP code [5] version 6. The MCNP code describes in detail the geometry of the neutron generator and simulates the neutron spectra resulting from all possible reactions occurring between the D/T (mono-atomic, bi-atomic etc) ions in the beam and the TiT/D target [6].

The present paper describes the neutron energy spectra obtained by employing high-resolution SCD neutron spectrometers. For the first time, we demonstrate the capability to accurately determine the detailed ion composition of the beam. This is made possible by exploiting the instrument's high energy resolution to discriminate the different reaction components that make up the whole neutron spectrum and that come from reactions between mixed D/T beam ions and T/D nuclei in the target. The result opens up new prospects for beam ion studies, and in general for neutron spectroscopy studies, in DT plasmas. An example that we have studied regards to the possibility of observing non classical beam slowing down in current drive studies at ITER using neutron spectroscopy.

2. Experimental setup and calibration procedure

2.1. Single crystal diamond detector

Artificial chemical vapour deposition SCD detectors have shown excellent performances in fast neutron spectroscopy due to their high energy resolution, fast time response and high radiation hardness [7–10] and are now being exploited for measurements of the 2.5 MeV neutron spectrum in deuterium plasmas at JET [11, 12]. Neutron detection in SCD is based on the collection of the electron–hole pairs generated by the slowing down of the charged particles produced by the interactions between neutrons and carbon nuclei. For 14 MeV neutrons the main reaction channels of interest are: elastic and inelastic scattering ^{12}C(n,n')^{12}C which features the highest cross section and gives rise to a continuum in the measured pulse height spectrum (PHS); the n-3α reaction ^{12}C(n,n')3α with a Q_{value} of -7.23 MeV; and the n-α reaction ^{12}C(n,α)^{9}Be with a Q_{value} of -5.702 MeV. The latter is the best candidate reaction for 14 MeV neutron spectroscopy, as it leads to a well-defined peak centred at $E_{dep} = E_n - 5.702$ MeV which provides a univocal one to one relation between incoming neutron energy and measured deposited energy. The shape of this peak is due to two independent contributions, namely the broadening due to the intrinsic resolution of the SCD itself and an additional kinematic broadening that depends on the energy distribution of the incoming neutron beam around 14 MeV. When the kinematic contribution dominates over the intrinsic broadening the shape of this peak becomes a diagnostic of the incoming 14 MeV neutron energy spectrum. The SCD neutron spectrometer used in these measurements was designed and built by the CNR-ISM institute in Rome (Italy) and is made of an artificial single-crystal chemical vapour deposition diamond sample ($4.5 \times 4.5 \times 0.5$ mm^3) grown by Element Six Ltd [13]. The Ohmic contacts on the top and bottom surfaces were obtained by subsequent sputtering deposition of a multilayer metal structure (patent pending), followed by a final gold layer deposition. In figure 1, the SCD is shown together with the dedicated 1 mm thick alumina printed circuit board (PCB) and the aluminium metal case. The latter is needed to shield the detector from electromagnetic interferences and to provide mechanical protection.

A dedicated custom electronic chain was used for these measurements (see figure 2). The detector was coupled to a CIVIDEC C6 fast charge preamplifier [14], which features a rise time of 3.5 ns and a shaping time of 25 ns. The preamplifier, supplied with a 12 V DC power supply has a bias current of 25 mA, a gain of 6 mV fC^{-1} and a bandwidth of 100 MHz. A CAEN [15] high voltage supply model NDT1470 was used to supply a voltage of $+400$ V to the detector, which corresponds to an average electric field of 0.8 V μm^{-1} in the bulk material. In some measurements, instead of the C6 model, a CIVIDEC CX preamplifier optimized for high-resolution spectroscopy was used. The latter has a rise time of 80 ns, a shaping time of 180 ns and a gain of 12 mV fC^{-1}. The preamplifier output
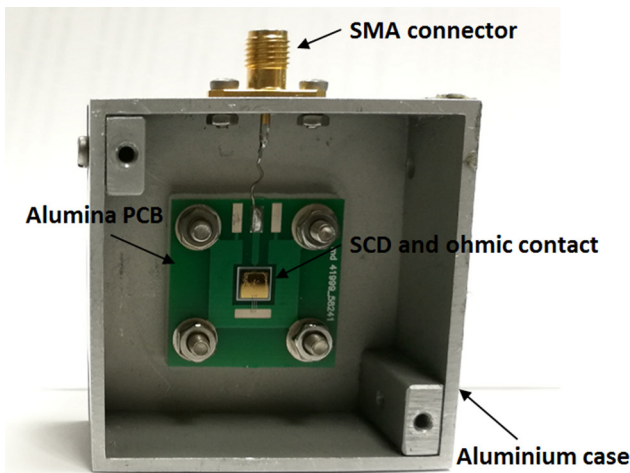
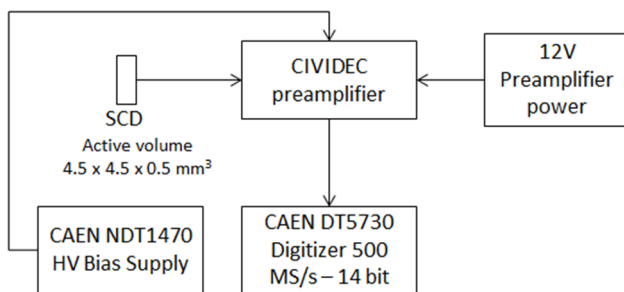**Figure 1.** Picture of the SCD detector.

Figure 2. Scheme of the SCD electronic chain.

was fed to an 8-channel waveform digitizer, CAEN DT5730. This is a 14-bit and 500 MSamples s^{-1}-rate digitizer equipped with CAEN software able to perform on-line measurements of the pulse area, by integrating each signal in a user defined gate, namely 40 ns for the C6 preamplifier and about 700 ns for the CX preamplifier. In some cases, the analog signal produced as output of the preamplifier was duplicated by a linear Fan-In Fan-Out module and simultaneously acquired with two different digitizers. The first was configured to digitize the full waveform corresponding to each detection event for offline analysis, while the second digitizer was set to process online each pulse from the detector, so to obtain energy/time list mode data.

The detector was placed on a rotating arm at different distances and angles to characterise the neutron energy emission spectra of the NGs (see figure 3).

2.2. Calibration procedure

Initially, the SCD was calibrated in the laboratory in vacuum with a ^{241}Am electro-deposited source which emits α particles with three different energies (5.486, 5.442, 5.388 MeV) with branching ratio (84.5%, 13.06%, 1.62%, respectively). On site, during the experiment, the calibration was verified with ^{241}Am electro-deposited source in air and correction factors due to the alpha particle energy loss in air were calculated and applied. The dominant factors that affect the accuracy of the α calibration in vacuum are connected to the energy straggling

of the α particles in the materials before reaching the active part of the detector, namely the Ohmic contacts of the diamond. It was found that the uncertainties in the knowledge of the SCD contact thicknesses limit the accuracy in the calibration to a few tens of keV, which is not sufficient for a detailed data analysis. For this reason, an iterative Bayesian calibration method based on prior assumptions has been implemented and is described below.

At the time of the measurements, the NG specifications provided by the supplier refer to a D/T mixture in the beam and in the target with nominal concentration at 50–50%. Instead, it was observed that D$^+$, T$^+$, D$_2^+$, T$_2^+$, DT$^+$, species were present in the beam, resulting in up to six observed different NG neutron energy distributions. This is due to the different kinetic energy of the species when they reach the T/D target. D$^+$ and T$^+$ ions are accelerated by the nominal NG operational voltage V_{op}. D$_2^+$ and T$_2^+$ molecules are accelerated by the same voltage and the individual atoms thus have half of the energy each. Finally, DT$^+$ ions split into a D$^+$ and a T$^+$ ions having 2/5 and 3/5 each of total energy, respectively. For this reason, a neutron source routine was developed in MCNP together with the detailed model of the generator [6, 16], producing the six neutron energy spectra resulting from all possible reactions occurring with the D/T ions in the beam impinging on the TiT/D target.

In previous experiments [7–9], the SCD was characterized, namely its resolution was measured at a neutron source to be equal to 120 keV FWHM at 14 MeV for the *n*-α reaction ^{12}C$(n,\alpha)^9$Be. In the case of the NG neutron calibration, the expected SCD pulse height spectra were thus obtained convoluting the simulated six neutron energy spectra with a Gaussian-shaped SCD response function of FHWM equal to 120 keV (as shown in figure 4). We observe that the six simulated neutron components provide pulse height spectra that cover deposited energy from 8.4 to 9.2 MeV.

The iterative Bayesian calibration method was performed on the neutron data recorded at zero degrees with respect to the beam direction. Zero degrees is the best angle since, due to the reaction kinematics, the six different neutron energy components are better separated in energy (see section 3.1). Furthermore, at zero degrees, the neutron energy uncertainty due to the angular uncertainty of the experimental setup is minimized due to neutron energy dependence on the cosine of the emission angle. The observed PHS (see figure 5 left) recorded at zero degrees features a complex shape in which the structures are due to three main reactions in ^{12}C: elastic scattering, ^{12}C$(n,n')3\alpha$ and ^{12}C$(n,\alpha)^9$Be. The most energetic peak (see figure 5 right) centred at ~8.8 MeV is due to the ^{12}C$(n,\alpha)^9$Be reaction and is the most useful one for neutron spectroscopy. We note that it features three characteristic structures caused by the different neutron energy components. The Bayesian calibration method we have used employs two calibration points to determine the relation between deposited energy and ADC channels. The first point is given by the neutron elastic scattering edge on ^{12}C which is at a well-defined position $E_{\text{edge}} = 0.284 * E_n$ while the second is obtained with *a priori* assumption on the first structure located at about 8.7 MeV in the PHS spectrum. A calibration curve is so
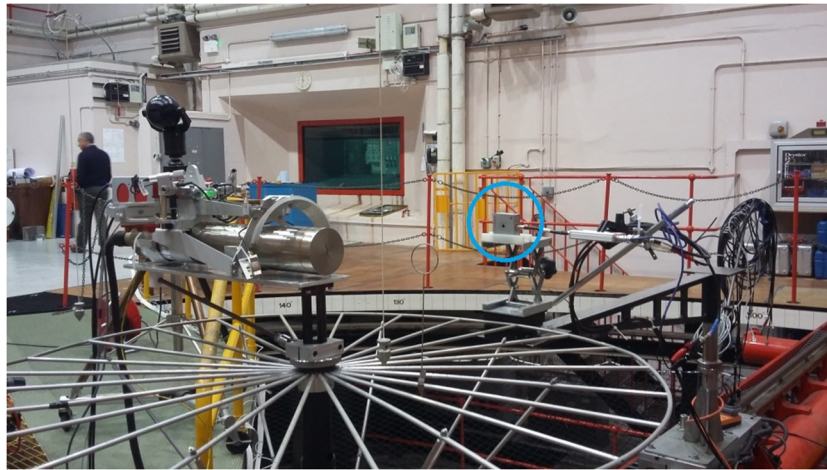
Figure 3. Experimental setup. The NG (on the left) is in the centre of a circular platform and the SCD (circled) at 90° with respect to the D/T beam direction in the NG.
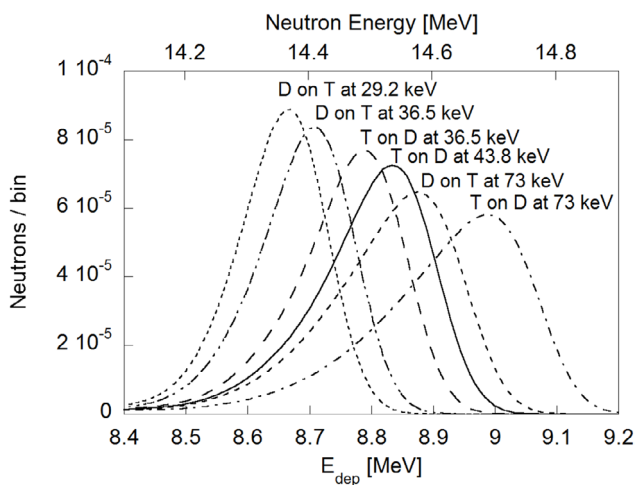

Figure 4. Theoretical normalized SCD pulse height spectra corresponding to each NG neutron emission component and resulting from the MCNP model. The SCD response function is assumed to be Gaussian-shaped of 120 keV FWHM. The lower *x*-axis represents the deposited energy inside the detector by neutrons. The upper *x*-axis represents the energy of the incoming neutrons.

obtained and used in a numerical fit between measured data and the six MCNP simulated neutron energy spectral components. The method is repeated for different *a priori* assumptions and the best agreement was obtained when the first structure of the figure 5 right is associated to the combination of the first two peaks of the figure 4, namely D on T at 29.2 keV and D on T at 36.5 keV. Other assumptions on the first structure in the PHS provided significantly worse Chi-square value.

In order to validate the iterative calibration method, a consistency check with the α particles calibration performed on site during the measurement was done and indicates that they are in agreement within $\pm 5\%$ uncertainty (see figure 6). Moreover, a second independent consistency check of the iterative calibration is given by the comparison between the measurement carried out at nominally 90° with respect to the incoming NG beam and the MCNP simulations (see figure 7). In this case the six neutron components overlap due to the

kinematics. It was found that the best agreement comes with the simulation at 84°, which is within the expected angular uncertainty due to the experimental-setup. We noted that on the low energy side of the peak of figure 7, the data show a low energy tail which does not overlap with the simulation. This is interpreted as due to neutron events that lead to a partial charge collection in the SCD.

3. Results and discussion

3.1. Study of the energy spectrum dependence on the emission angles

The SCD neutron spectrometer was placed on a rotating arm at different distances exploring the neutron energy spectrum dependence on the neutron emission angle for the NG. Neutron energy spectra have been recorded at different angles from 0 to 150° with respect to the beam direction. Figure 8 shows the anisotropy of the neutron emission intensity which is due to the reaction kinetics. The evaluation of the anisotropy profile of the neutron emission rate was a key aspect in the NG calibration in order to derive the total neutron emission in 4π. In particular, as shown in detailed in [4], the neutron emission rate as a function of the angle has been studied by using calibrated long counter detectors and activation foils. Furthermore, as shown in figure 8, the neutrons emitted at zero degrees exhibit a broader spectrum than at other angles, because of the reaction kinetics. In particular, the broadening of the spectra decrease from 0 to 90° and then it increases again from 90 to 150°. This is due to the six different neutron energy components which are well separated at zero degrees and overlap at 90°.

3.2. Analysis of the beam composition

The aim of the analysis is to resolve the complex features of the neutron energy spectra resulting from the mixed D/T beam ions reacting with the T/D nuclei present in the target. The analysis is based on the numerical fitting of the simulated neutron components resulting from the five ion species convolved
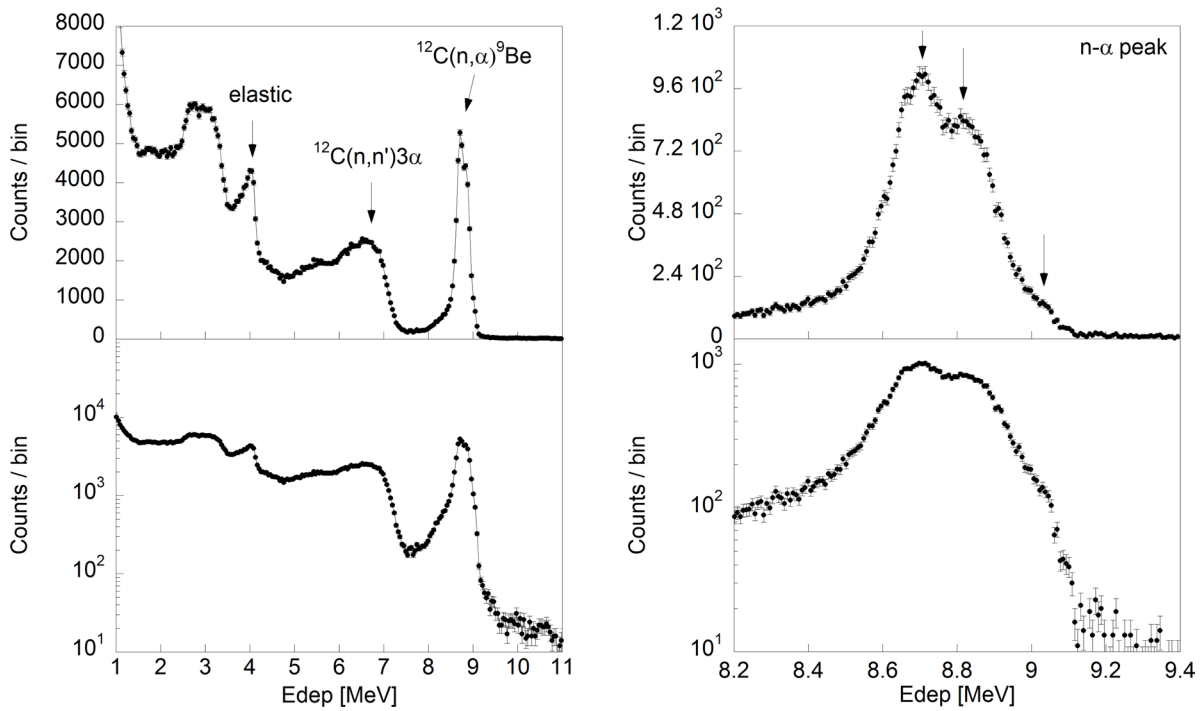
Figure 5. PHS recorded at zero degrees in linear scale (top-left) and logarithmic scale (bottom-left). The *n*-α peak is shown in detail in linear scale (top-right) and in logarithm scale (bottom-right). The arrows in the plot indicate the main structures in the PHS spectrum and the structures of the peak. $E_{peak} = E_n - 5.702$ MeV.
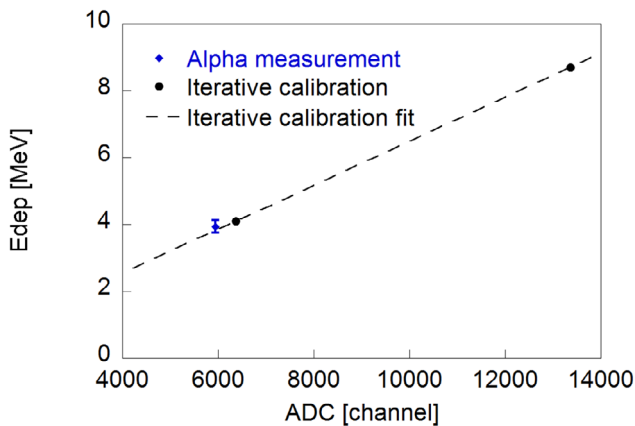

Figure 6. Calibration fit based on the iterative calibration process shown with the ^{241}Am calibration point.
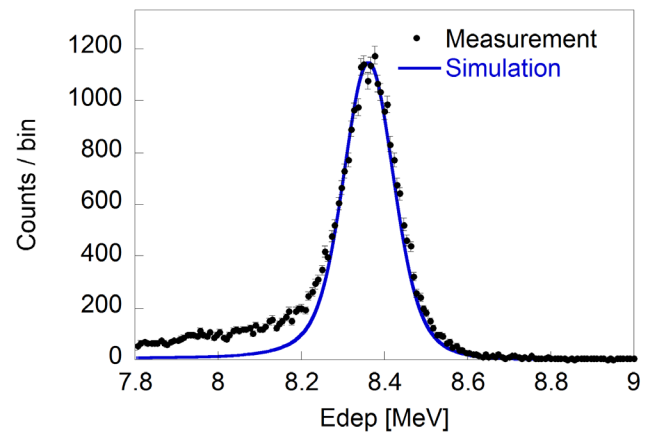

Figure 7. Comparison between the PHS measured at nominally 90° and the simulation at 84°.

with the SCD response function to the experimental data taken at zero degrees. In addition to the model components displayed in figure 4, an MCNP calculation [16] has been performed to determine the absolute neutron yield related to each component. Figure 9 shows the best 5-free parameters numerical fit of the data, together with the neutron contributions of the five ion species weighted to the neutron yield. Here the neutron components due to the reaction D on T at 29.2 keV and T on D at 43.8 keV (see figure 4) were added together and considered as a single DT component. The goodness of the fit is assessed on the reduced Chi-square value which results to be equal to 1.50. This indicates that the analysis model used for the data fit provides a good description of the SCD data. Looking at the figure 9, it can be noticed that the DT component is the dominant one and it is the one responsible for the

'*double*' peak structure. The T component (T on D at 73 keV), instead, is the most energetic one and it is the only one that can describe the high energy tail of the peak. Table 1 summarizes the calculated neutron yields of each component and the estimated incident particle beam composition, respectively. The dominant fraction of the incident beam is represented by the DT molecules (~80.4%) followed by D_2 and T_2 molecules (~9% and 7.3% respectively), T ions (~2.7%) and finally by D ions (~0.6%). The errors in table 1 represent the statistical uncertainties of the parameters based on the covariance matrix resulting from the Chi-square minimization in the fit procedure and they include the effect of correlations with the other parameters. The analysis has been performed by using the software framework ROOT [17]. In figure 10 the fit results are shown together with the 95% of confidence interval of the fit.
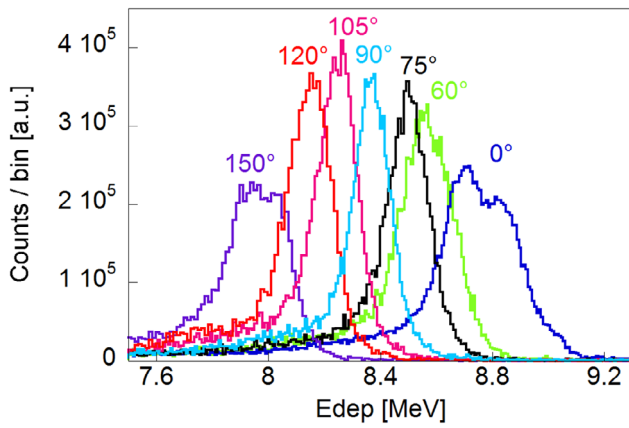
Figure 8. Recorded pulse height spectra measured by the SCD at different angles from 0 to 150°. The *x*-axis represents the deposited energy in detector.
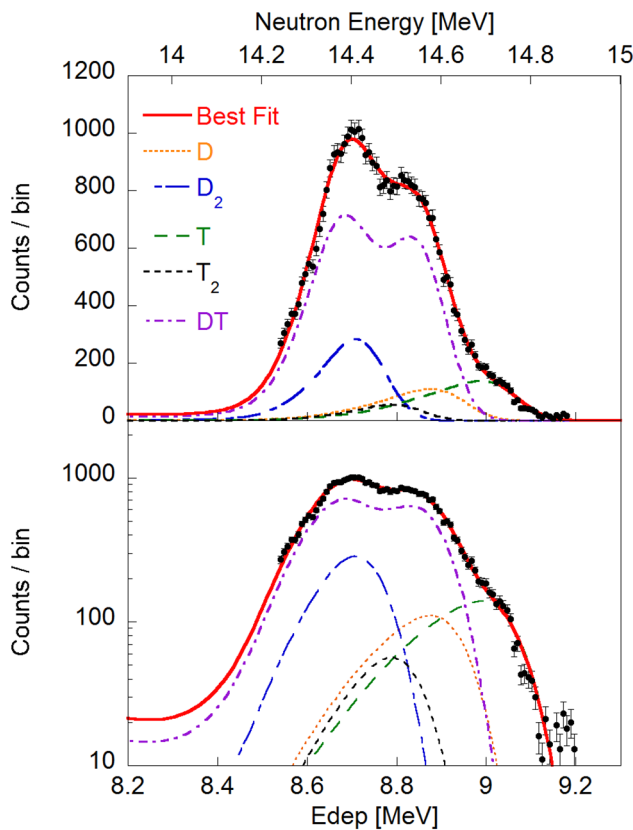

Figure 9. SCD PHS at 0° shown as black dots without the low energy tail due to partial charge collection (see text). The neutron beam components with their weights and their sum correspond to the best fit to the data. The lower *x*-axis represents the neutron deposited energy inside the detector while the upper *x*-axis represents the energy of the incoming neutrons. The *y*-axis of the graph in the top is given in linear scale, whereas in the bottom graph the *y*-axis is given in logarithmic scale.

These results demonstrate the capability of SCD to determine the beam composition in a mixed DT beam and could be applied on the neutral beams injected in thermonuclear fusion experiments. This was demonstrated in an earlier work [18], where the main features of the neutron spectrum have been

Table 1. Summary of the neutron yields of each D/T beam component and the estimated incident particle beam composition derived by the best numerical fit.

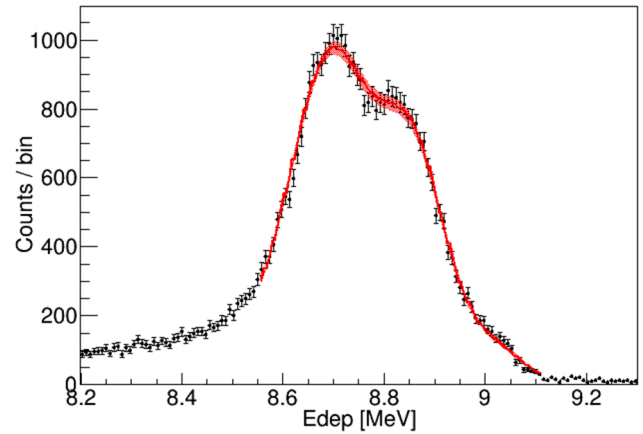| Incident particle beam composition	Neutron yield	Concentration (%)
DT$^+$	2.60×10^{-7}	80.4 ± 6.1
D$_2^+$	2.79×10^{-6}	9 ± 0.9
T$_2^+$	6.59×10^{-8}	7.3 ± 2.5
T$^+$	1.37×10^{-6}	2.7 ± 0.2
D$^+$	3.85×10^{-6}	0.6 ± 0.1

Figure 10. SCD PHS at 0° shown with the best fit of the data together with its 95% confidence interval (red band).

observed on the JET tokamak with a mixed D/T beam used to heat the plasma.

4. New prospects for diagnosing DT plasmas

The unprecedented intrinsic energy resolution <1% of diamond detectors for 14 MeV neutrons opens up new prospects for diagnosing DT plasmas as demonstrated with the detailed analysis of the NG D/T beam composition. In this work we also explore the possibility to use SCDs to study the non-classical slowing down of the beam ions in ITER DT plasmas. As in [8], where this phenomenon was studied for JET, here we apply the analytical formulas of Gaffey [19] to determine the steady-state distribution function $f_b(v)$ of a beam of neutral ions that slows down in an ITER DT plasma due to Coulomb collisions. Following [8], we also introduce a term $L(f)$ in Gaffey's equation which heuristically describes an additional, non-classical ('anomalous') loss mechanism acting on the beam ions. $L(f)$ is given by

$$L(f) = \frac{f_b}{k\tau_s}\left(\frac{v_b}{2v}\right)^\alpha = \frac{f_b}{\tau_\alpha(v)}. \quad (4.1)$$

Here v_b and τ_s represent the initial velocity and the Spitzer slowing down time, respectively. For $v = v_b/2$, the velocity dependent slowing down time $\tau_\alpha(v)$ implied by equation (4.1) is equal to $k \cdot \tau_s$ and the magnitude of k determines the ratio between the classical and anomalous time scales. The exponent α, instead, controls the effect of the anomalous losses on
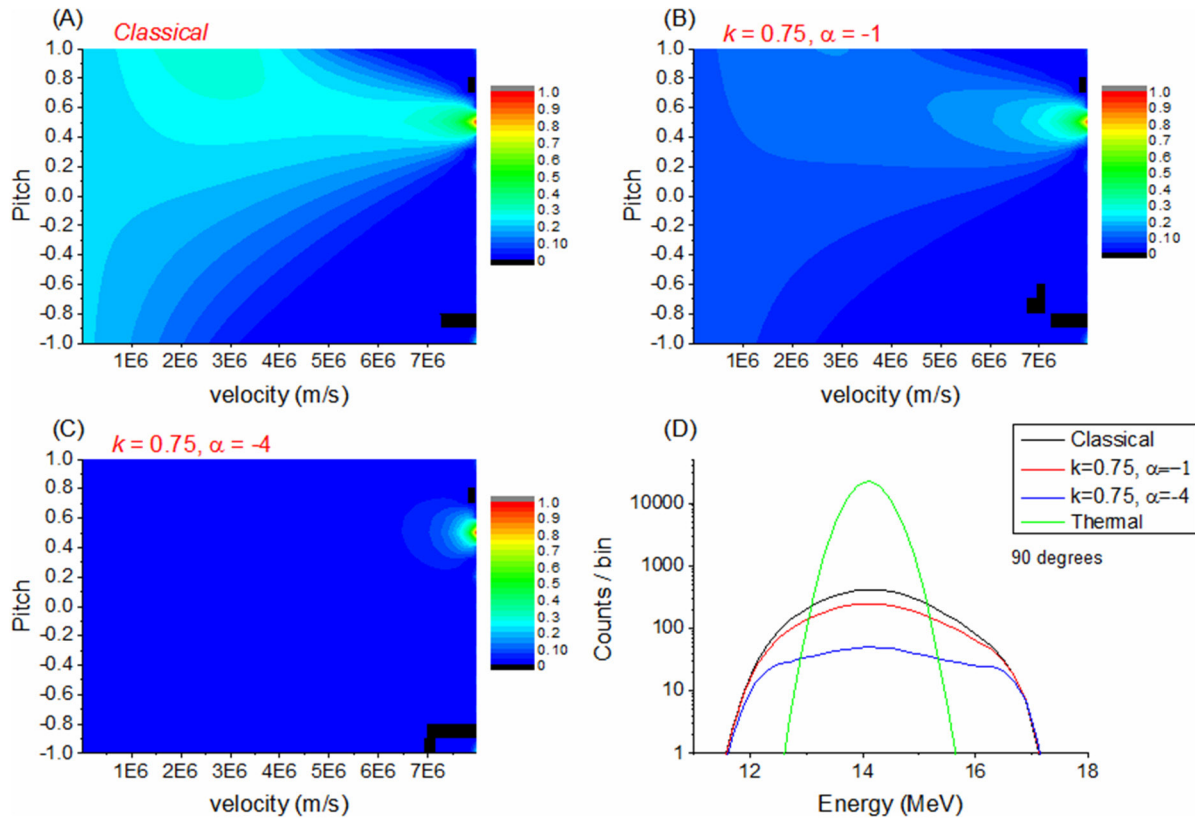
Figure 11. Calculations of the slowing down distributions of 1 MeV NB tritons in hypothetic DT plasma in ITER (ion temperature and electron temperature equal to 20 keV; deuterium and tritium densities equal to $1.0 * 10^{20}$ m^{-3}). The classical solution (A) is compared to the anomalous cases (B) and (C) with $k = 0.75$, $\alpha = -1$ and $k = 0.75$, $\alpha = -4$, respectively. In panel (D), the relative neutron energy spectra (viewed at 90°) generated by the NB tritons and the bulk thermal D (20 keV) plasma are shown, together with the neutron energy spectrum emitted by thermal bulk DT plasma at 20 keV. The neutron energy spectrum corresponding to the classical case contains 5000 events. The FWHM of these three components is 2.3 MeV, 2.6 MeV and 3.6 MeV in cases of classical, $k = 0.75$, $\alpha = -1$ and $k = 0.75$, $\alpha = -4$ slowing down, respectively.

ions at different velocities so that, for example, if $\alpha < 0$ ions with velocities $v > v_b/2$ are preferentially lost.

As shown in [8, 19], equation (4.1) can be solved by standard numerical techniques. The results obtained for an hypothetical ITER neutral beam injection (NBI) scenario in which tritons are injected with energy $E_b = 1$ MeV and pitch angle of 0.5 into a DT plasma (with ion and electron temperature of 20 keV and deuterium and tritium density of 1.0×10^{20} m^{-3}) are shown in figure 11 for three different cases (A–B–C). The classical solution (A) is compared to the anomalous cases (B) and (C) with $k = 0.75$, $\alpha = -1$ and $k = 0.75$, $\alpha = -4$, respectively. For the classic case (figure 11(A)), the ions distribution features a clear anisotropy in the injection energy region. For lower energies instead, the slowing down distribution becomes more isotropic due to the pitch angle scattering caused by collision with bulk ions. When the classic solution is compared to the anomalous cases (figure 11(B)) we note that the anisotropic part is almost unaffected by the loss term $L(f)$, whereas the low energy distribution is less pronounced. This is emphasized in the anomalous slowing down case (figure 11(C)) in which the isotropic distribution at low energies almost disappears due to a lower value of the α exponent which rules the ions dispersion.

Using as input the above simulated tritons velocity distribution, Monte Carlo simulations based on GENESIS code [20] were performed to calculate neutron energy spectra, assuming to have D bulk thermal plasma at 20 keV temperature (see figure 11). Figure 11(D) shows the calculated neutron energy spectra generated by the three NBI distribution cases interacting with the thermal D plasma, together with the thermal bulk DT plasma component (20 keV). Here, the latter is shown as dominant contribution. The thermal component on ITER, in fact, is expected to be between 90% and 95% with respect to the NBI one [21].

In order to study the diagnostic capabilities of the SCD, the classical and the anomalous components viewed from two different angles, together with the thermal contribution, have been convolved with the diamond response function. Figure 12 shows the results in terms of ^{12}C$(n,\alpha)^9$Be peak at 90° (top panel A) and 45° (bottom panel B), respectively. The exhibited spectra were normalized in order to have 5000 counts in the classic NBI component whereas in the anomalous cases the number of counts in the NBI components scales with the associated dispersion factor. A counts number equal to 5000 has been chosen according to the expected neutron flux (10^9 n/cm^2/s) at the high-resolution neutron spectrometer (HRNS) position [22]. In fact, by considering the diamond efficiency to 14 MeV neutron to be of about 5×10^{-4} in
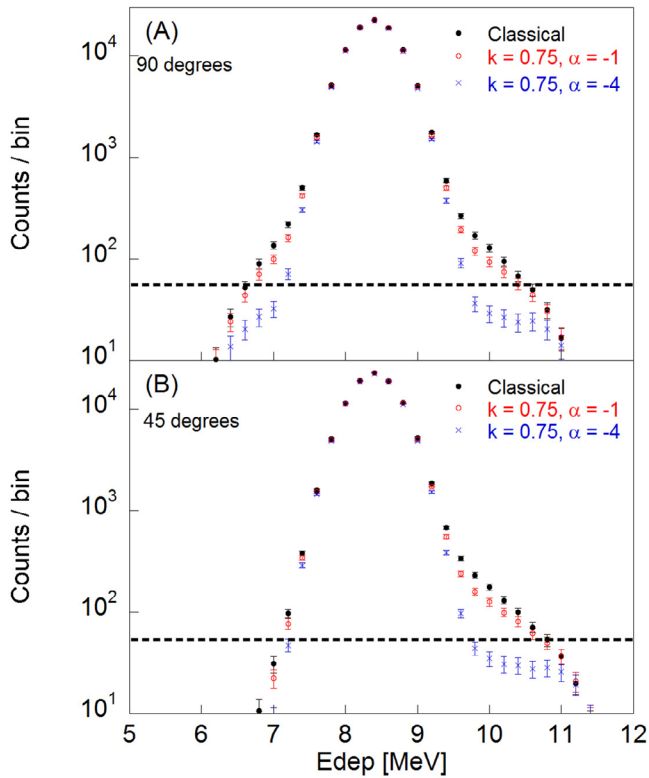
Figure 12. Comparison of the neutron spectra in terms of $^{12}C(n,\alpha)^9$Be peak for the three studied cases after the convolution with diamond response function. The dashed lines represent the level of sensitivity of the SCD. Panel (A) and (B) show the neutron spectra viewed at 90° and 45°, respectively. The y-axis of both the graphs is shown in logarithmic scale.
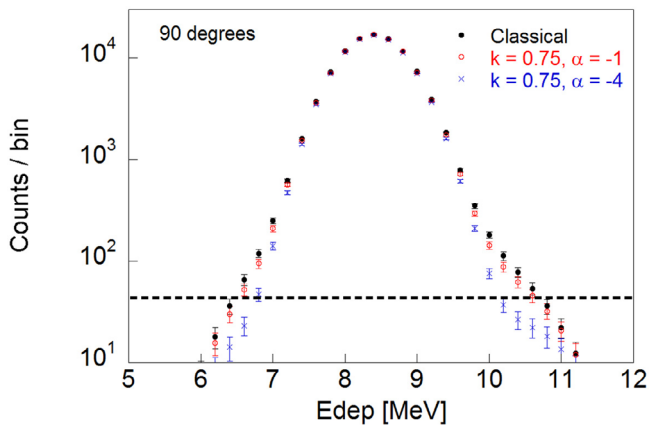

Figure 13. Comparison of the neutron spectra viewed at 90°, in terms of $^{12}C(n,\alpha)^9$Be peak for the three studied cases after the convolution with a neutron spectrometer with energy resolution equal to 5% at 14 MeV. The dashed line represents the level of sensitivity of the detector. The *y*-axis is shown in logarithmic scale.

the *n*-α peak and the active area of a 12 pixel SCD matrix [7, 10], we can estimate to have on ITER roughly 5000 counts per half second in the classic NBI component at the HRNS position. Consequently, this number is comparable to the number of counts that we can have by integrating for the 1 MeV NB tritons slowing down time, therefore allowing NBI diagnosing. The spectra display a dominant thermal component of about 0.8 MeV FWHM and additional high and low

energy tails induced by NBI heating at an amplitude of about 10^{-2} compared to the peak from thermal emission. Compared to the classical slowing down case, the effects of an additional anomalous loss of the beam ions are distinguishable as deviations in the high energy tails of the spectrum at a level above 5×10^{-3} with respect to the main peak. This can be observed with today's sensitivity limit of SCDs. The deviation is better observed at 45° and for the $k = 0.75$, $\alpha = -4$ case.

In order to study the importance of the high energy resolution enabled by SCDs, in figure 13 we consider the case of an SCD with a poorer energy resolution of 5% at 14 MeV and that views the plasma along a line of sight at 90° with respect to the magnetic field. The dominant thermal DT neutron component has a 1.1 MeV FWHM and the contribution of the NBI component can be separated from the thermal peak at deposited energies $E_d > 10$ MeV. When compared to figure 12(A), the spectra have smoother gradients, which makes it harder to observe differences among the classical, $k = 0.75$ $\alpha = -1$ and $k = 0.75$ $\alpha = -4$ cases. The poorer energy resolution results also in a significantly broader spectrum for which the separation of the Thermal and NBI components becomes more difficult.

5. Conclusions

The NGs selected for the JET neutron calibration have been fully characterized and calibrated at the Neutron Metrology Laboratory of the National Physical Laboratory (NPL, Teddington, UK). The unprecedented intrinsic energy resolution (<1% FWHM at 14 MeV) of the SCD neutron spectrometer made possible to resolve for the first time the complex features of the neutron energy spectra resulting from the mixed D/T beam ions reacting with the T/D nuclei present in the target. The dominant NG beam component was found to be the DT molecule. As demonstrated with the detailed analysis of the NG D/T beam composition, the SCDs open up new prospects for diagnosing of DT plasmas, such as for example the studied heuristic case of a non-classical slowing down of the beam ions on ITER DT plasmas. The simulations performed indicate that the diamond detectors would provide good separation of the different neutron components and that information on the NB slowing down can be achieved.

Acknowledgments

ORCID iDs

D Rigamonti ⬥ https://orcid.org/0000-0003-0183-0965
M Nocente ⬥ https://orcid.org/0000-0003-0170-5275

References

[1] Syme D B *et al* 2014 Fusion yield measurements on JET and their calibration *Fusion Eng. Des.* **89** 2766–75

[2] Batistoni P *et al* 2016 Technological exploitation of deuterium–tritium operations at JET in support of ITER design, operation and safety *Fusion Eng. Des* **109–11** 278–85

[3] VNIIA 2017 www.vniia.ru

[4] Batistoni P *et al* 2018 14 MeV Calibration of JET neutron detectors—Phase 1: calibration and characterization of the neutron source *Nucl. Fusion* **58** 026012

[5] MCNP 2018 www.mcnp.lanl.gov/

[6] Cufar A *et al* 2017 Calculations to support JET neutron yield calibration: modelling of neutron emission from a compact DT neutron generator *Nucl. Instrum. Methods Phys. Res.* A **847** 199–204

[7] Rigamonti D *et al* 2005 Capabilities of a diamond detector matrix for neutron spectroscopy measurements at JET *PoS(ECPD2015)*

[8] Giacomelli L *et al* 2016 Neutron emission spectroscopy of DT plasmas at enhanced energy resolution with diamond detectors *Rev. Sci. Instrum.* **87** 11D822

[9] Rebai M *et al* 2016 Response function of single crystal synthetic diamond detectors to 1-4 MeV neutrons for spectroscopy of D plasmas *Rev. Sci. Instrum.* **87** 11D823

[10] Muraro A *et al* 2016 First neutron spectroscopy measurements with a pixelated diamond detector at JET *Rev. Sci. Instrum.* **87** 11D833

[11] Cazzaniga C *et al* 2014 Single crystal diamond detector measurements of deuterium-deuterium and deuterium-tritium neutrons in Joint European Torus fusion plasmas *Rev. Sci. Instrum.* **85** 043506

[12] Nocente M *et al* 2015 Fast ion energy distribution from third harmonic radio frequency heating measured with a single crystal diamond detector at the Joint European Torus *Rev. Sci. Instrum.* **86** 103501

[13] Element Six 2018 www.e6.com/en/Home

[14] Cividec 2018 www.cividec.at/

[15] Caen 2018 www.caen.it/

[16] Cufar A *et al* Modelling of the neutron production in the mixed beam DT neutron generator submitted to *Fusion Eng. Des.* 2017

[17] ROOT 2018 https://root.cern.ch/

[18] Hellesen C *et al* 2015 Fuel ion ratio determination in NBI heated deuterium tritium fusion plasmas at JET using neutron emission spectrometry *Nucl. Fusion* **55** 023005

[19] Gaffey J D 1976 Energetic ion distribution resulting from neutral beam injection in tokamaks *J. Plasma Phys.* **16** 149

[20] Tardocchi M *et al* 2011 Spectral Broadening of Characteristic γ-Ray Emission Peaks from 12C(3He,pγ)14N Reactions in Fusion Plasmas *Phys. Rev. Lett.* **107** 205002

[21] Eriksson L-G *et al* 2007 *Report on the Task: ICRF, NBI and ITER Diagnostics* TW6-TPDS-DIADEV (Istituto di Fisica del Plasma "P. Caldirola")

[22] Scholz M *et al* 2016 System design description document (DDD) *High Resolution Neutron Spectrometer DDD-PBS 55.BB (Enabled) (22 July 2016)*

[23] Litaudon X *et al* 2017 Overview of the JET results in support to ITER *Nucl. Fusion* **57** 102001